Lasers in Manufacturing Conference 2021

Remote laser welding of die casting aluminum parts for automotive applications with beam oscillation and adjustable ring mode laser

Mikhail Sokolov[a,*], Pasquale Franciosa[a], Dariusz Ceglarek[a]

[a] *WMG, University of Warwick, Coventry CV4 7AL, UK*

Abstract

Aluminum die casting alloys are frequently used in the automotive industry for front and rear rails, corner nodes and interface blocks to weld together varying cross sections of aluminum extrusions in lightweight chassis structures. However, these materials have limited weldability due to entrapped gases which generate pores or cavities. Therefore, the thermal cycle during welding as well as the overall heat balance need to be carefully controlled in order to reduce the porosity level and hence achieve the desired joint integrity. This paper focuses on the selection of process parameters for the material combination of Al die casting C611 to Al extrusion AA6063. Results showed that the porosity level can be significantly reduced from 5-6% to below 2% of the weld area through the combination of beam oscillation and dual beam welding with Adjustable Ring Mode laser. Additionally, the selected parameters resulted in an average ultimate tensile strength of 120 MPa.

Keywords: Remote Laser Welding; Die Casting Aluminium Welding; Weld Porosity Control; Beam Oscillation; Adjustable Ring Mode Laser

1. Introduction

The drive towards electrical powertrain and EV adoption (Kumar and Alok, 2020) has spearheaded the need for optimized light-weight structures for automotive body applications. An example of such a solution is the automotive body designed from aluminum extrusions with varying cross sections, welded together via cast

* Corresponding author. Tel.: +44(0) 7576410561 .
E-mail address: mikhail.sokolov@warwick.ac.uk .

aluminum nodes; or upper structural assemblies made of vacuum high pressure die casting aluminum to reduce their thickness.

Recent studies (e.g. Hong and Shin, 2017; Gullino et al., 2019) have shown clear advantages of applying laser welding in joining light-weight aluminum alloys for automotive industry. Increasingly, remote laser welding (RLW) is seen as a potential solution to provide high welding speed; flexibility due to non-contact single-side access with no need for shielding gas or filler wire (Ceglarek et al., 2015). Franciosa et al., 2019 and Sun et al., 2020 investigated the application of laser beam oscillation for welding aluminium alloys in fillet lap welding setup as the benefits of switching from overlap seam welding provides weight saving of up to 4.5 kg per car. Fillet lap welding setup also enables in-process gap bridging – which is critical for long continuous welds.

However, there are several challenges pertaining to RLW applications for joining aluminum alloys and in particular casting alloys due to high level of porosity formation during RLW process, influenced by two main factors:

- Metallurgical-related: entrapped gases, mostly hydrogen;
- Joining-related: laser welding process instability, as rapid keyhole closing entraps the occluded gases.

Different methods have been proposed to reduce the porosity level in RLW of die casting aluminum, focused on releasing the hydrogen from the weld pool and stabilization of the keyhole. Dittrich et al., 2017 studied the effect of beam oscillation on stabilization of the keyhole, which resulted in improved degasification of the molten pool. A stable keyhole leads to a stable surface with less spattering and, therefore, reduces the porosity. Stabilization of the keyhole during laser welding of aluminum in dual beam welding was reported by Maina et al., 2018. Coherent Inc. introduced a new concept of dual beam laser welding, called the Adjustable Ring Mode (ARM) laser with the key principle of independent control of power distribution in the inner core laser beam and outer ring-shaped laser beam. While the core beam stimulates the opening of the keyhole, the ring-shaped beam allows controlling the distribution of heat and cooling rate in and around the molten pool. Wang et al., 2020 has confirmed a positive effect of ARM laser on keyhole stabilization.

The present research aims at studying the combined effect of laser beam oscillation and dual beam welding with Adjustable Ring Mode laser distribution with the goal to reduce the porosity formation in commercially available die casting aluminum alloy. Results are presented for Al die casting C611, welded to Al extrusion AA6063 in fillet lap joint setup. These two alloys are commonly used in automotive industry for the fabrication of corner nodes, front and rear rails and engine shock towers.

Nomenclature

A_p	Porosity area, %
A_y	Laser beam oscillation amplitude, mm
A_z	Focal point position offset, mm
D_p	Pore diameter, mm
f	Oscillation frequency, Hz
IQR	Interquartile range
O_y	Laser beam lateral offset, mm
$P_{c,i}$	Laser power at core beam in point i, kW
$P_{r,i}$	Laser power at ring beam in point i, kW
S_x	Welding speed in x-axis direction, mm/s
tpa	Total pore area, mm^2
wpa	Weld pool area, mm^2

2. Experimental configuration and setup

2.1. Materials and equipment

The experiments were conducted using Al die casting alloy C611 and Al extrusion AA6063 described in Table 1. Dissimilar materials were welded by CW multi-mode Coherent fiber laser HighLight FL-ARM 10000 in fillet lap joint welding setup illustrated in Fig. 1. A list of equipment and parameters is shown in Table 2. All experiments were performed without shielding gas and without filler wire. Samples were wiped with acetone before welding to remove surface contaminations. For all C611 samples X-ray examination according to ASTM E 505 was performed to exclude the probability of pore formation during welding process, caused by initial pores in the material.

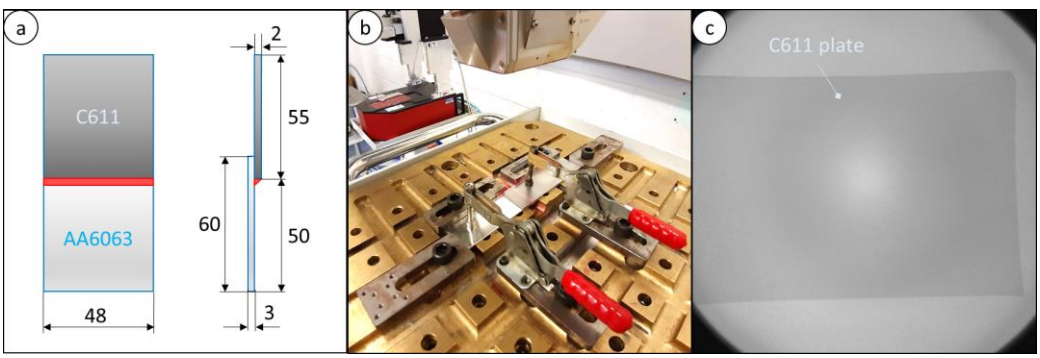

Fig. 1. Experimental setup: (a) weld joint geometry, (b) laser welding setup, (c) example of X-ray examination of C611

Table 1. Alloying composition of tested materials

Chemical composition, max wt. %	Si	Fe	Cu	Mn	Mg	Cr	Zn	Ti
C611	6.90	0.12	0.00	0.60	0.23	0.00	0.00	0.06
AA6063	0.45	0.50	0.11	0.10	0.60	0.1	0.00	0.15

Table 2. Specification of welding setup

HighLight FL-ARM	Units	Core	Ring
Nominal output power	W	5000	5000
Optical fibre diameter	µm	70	180
Spot diameter at focus	mm	0.14	0.36
Rayleigh length	mm	4.2	4.2
Welding optics: YW52 WeldMaster, Precitec GmbH			
Collimating length	mm	150	
Focusing length	mm	300	
Emission wavelength	nm	1080	

2.2. Methods

After welding, the samples were cut in three places: 7 mm from the weld start, middle of the weld and 7 mm from the weld end. Once the samples were extracted and polished the cross sections were photographed using Nikon Eclipse 150VN microscope in black-an-white mode. The pores were recognized on the cross-section photographs using an automatic pore recognition code developed in Matlab© as shown in Fig. 2. The approach is based on an edge detection algorithm which recognizes the closed boundaries (red circles in Fig. 2) of the pores; the total pore area counts the number of pixels, scaled in mm, inside the closed boundary.

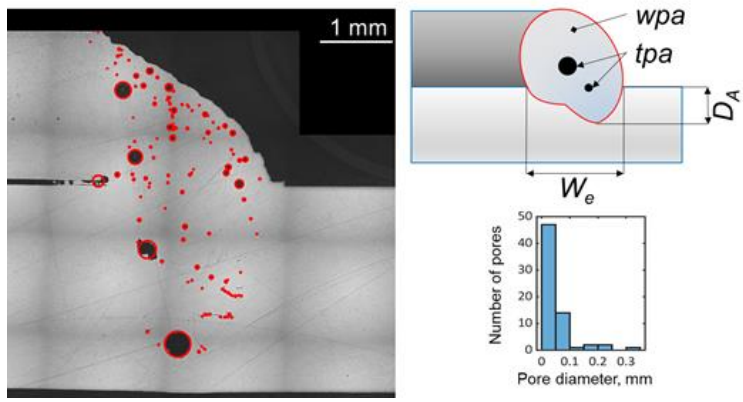

Fig. 2. Sample processing and automatic pore recognition using Matlab©

The key weld indicator was defined as porosity area (A_p). A_p indicates the percentage of the weld pool area covered with porosity and calculated as follows:

$$\mathrm{Ap} = \frac{tpa}{wpa} \tag{1}$$

where:

- *tpa* – total pore area, mm^2;
- *wpa* – weld pool area, mm^2.

The effective weld width (W_E) was measured at the interface between the two sheets, while the penetration depth (D_A) was measured as the depth into the lower sheet from the interface. Total pore area (*tpa*) was identified automatically using the Matlab© code; whereas, the weld pool area (*wpa*) was manually identified for each cross-section.

On completion of the metallographic examination, chosen experiment was repeated for tensile tests. Using 30KN Static Instron tensile machine at elongation rate of 10 mm/min, three replications were performed.

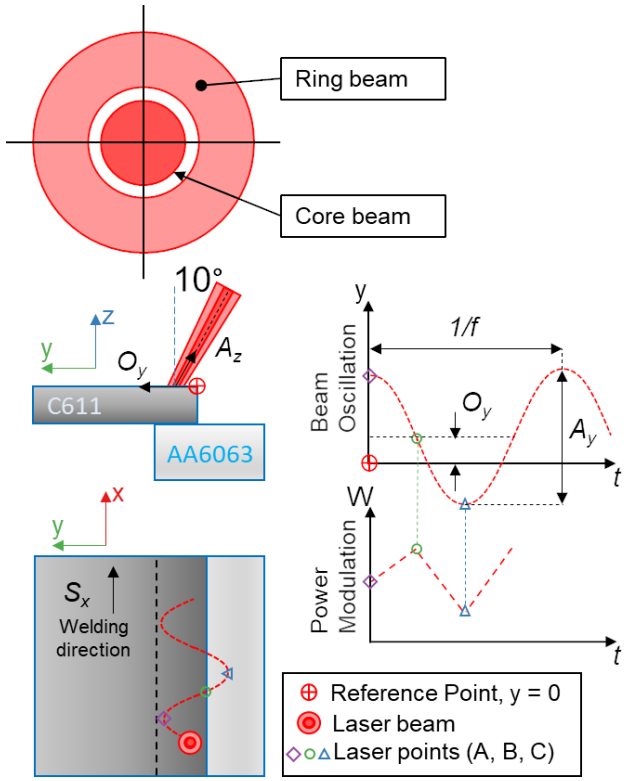

Fig. 3. Illustration of laser beam oscillation method with Adjustable Ring Mode (ARM) laser

In order to ensure both the extension of the melting pool and to reduce the probability of pore formation, high frequency beam oscillation with power modulation method was applied. The principle of the laser beam oscillation and power modulation method is shown in Fig. 3.

The following process parameters are used:

- $P_{c,i}$ – laser power of core beam, modulated transversally to the welding direction on three points: on the upper part (A), reference point (B) and lower part (C);
- $P_{r,i}$ - laser power of the ring beam, not modulated;
- f - oscillation frequency;
- A_y – oscillation amplitude;
- O_y - is measured from the reference point, and defines the position in the y direction of the laser beam the zero-position of A_y;
- A_z - focal point position offset;
- S_x – laser welding speed was constant at 66.67 mm/sec (4 m/min);
- Laser incident angle was fixed at 10°;
- All experiments were performed at zero gap.

2.3. Design of experiments

The experiments were focused on investigation of the effect of selected welding process parameters and analysis of their influence on A_p with 3^3 full factorial design. The experiments are summarized in Table 3. Three welding parameters were chosen:

- Frequency (f) – frequency beam oscillation above 100 Hz with the aim to facilitate the stirring effect that increases the keyhole stability and degasification of the molten pool;
- Power at ring beam (P_r) – to control the distribution of heat and cooling rate in and around the molten pool for keyhole stabilization;
- Focal offset (A_z) – to control the distribution of the spatial energy input;

Constant welding parameters were chosen to ensure the minimum weld penetration depth (D_A) of 1.2 mm – 40% of the bottom plate at zero gap between the plates.

Table 3. Experimental parameters, factors and levels

Constant welding parameter	Value		
$P_{c,A}$, W	2500		
$P_{c,B}$, W	4000		
$P_{c,C}$, W	2750		
O_y, mm	0		
S_x, mm/s	66.67		
Factors and levels			
Factor	Level 1	Level 2	Level 3
P_r, W	1000	1500	2000
A_z, mm	-2	0	2
f, Hz	100	150	200

3. Results and discussion

3.1. Metallographic examination

The experimental set examined the impact of three process parameters on the quality of the weld. Fig. 4 illustrates the effect of welding parameters on the porosity area (A_p). Results of the experiments, showing average values for weld geometry and porosity outputs, are reported in Table 4. Values of A_p below 2% are highlighted in bold. The spread of Ap along the weld is indicated by interquartile range (IQR) of 3 cross sections.

It can be seen from the data in Table 4 that even though experiment 11 shows the lowest A_p (1.5% in average: 1.9%, 1.7%, 0.8%), the average *tpa* (0.1244 mm^2) is almost the same as in experiment 24 (0.1249 mm^2) with similar result for A_p (1.6% in average: 1.1%, 2.1%, 1.5%). In addition, experiment 24 shows the lower spread for A_p (IQR 1.00) compared to experiment 11 (IQR 1.06) indicating that the process is stable along the weld. Important to notice that full penetration in experiment 11 (2.83 mm in average: 3.00 mm, 3.00 mm, 2.48 mm) significantly raises the risk of macrocracks on the bottom of the weld similar to that of experiment 3, shown in Fig. 4 (P_r = 1000 W, A_z = -2 mm, f = 100 Hz). Therefore, experiment 24 with partial penetration (2.14 mm in average: 2.37 mm, 2.20 mm, 1.84 mm) was chosen for further tensile testing.

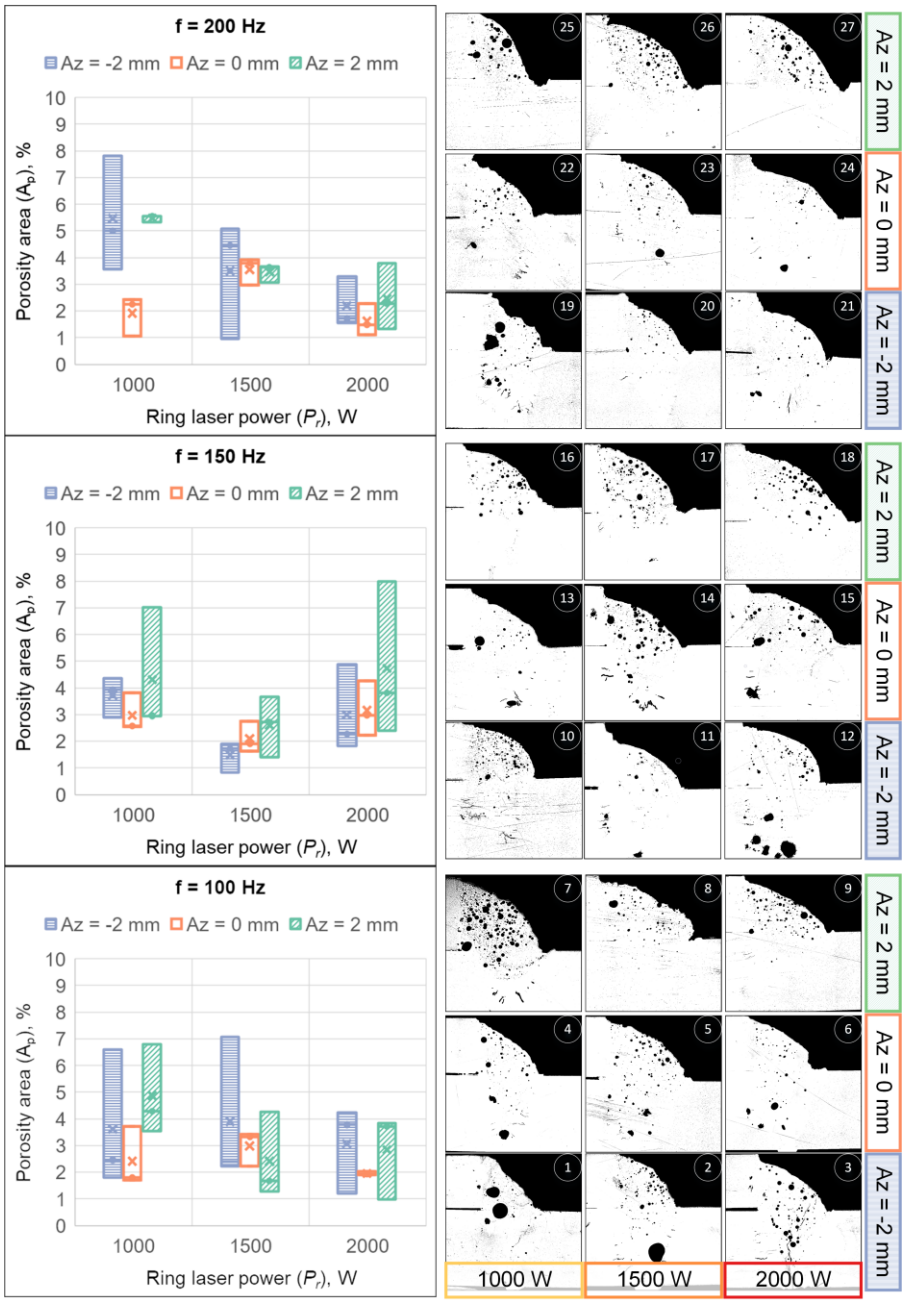

Fig. 4. Experimental results: box plots of porosity area A_p (left) and representative cross sections (right) at different levels of frequency (f), focal point position offset (A_z) and ring laser power (P_r)

Table 4. Experimental results: welding parameters, geometry and pores

Experiment	**Welding parameters**			**Geometry and pores, average**					
	P_r, W	A_z, mm	f, Hz	D_A, mm	We, mm	tpa, mm^2	A_p, %	A_p, IQR	max D_p, mm
1	1000	-2	100	3.00	2.45	0.2670	3.6	4.79	0.3316
2	1500	-2	100	3.00	2.49	0.3307	3.9	4.85	0.3257
3	2000	-2	100	3.00	2.81	0.3032	3.1	3.04	0.1690
4	1000	0	100	2.00	2.57	0.1843	2.4	2.02	0.2065
5	1500	0	100	2.28	2.88	0.2441	3.0	1.19	0.2848
6	2000	0	100	2.97	2.82	0.1751	2.0	0.13	0.2110
7	1000	2	100	1.60	2.71	0.3624	4.9	3.24	0.3157
8	1500	2	100	1.40	2.98	0.1878	2.4	2.98	0.2284
9	2000	2	100	1.74	3.04	0.2165	2.9	2.86	0.2519
10	1000	-2	150	2.02	2.62	0.3422	3.7	1.47	0.2544
11	**1500**	**-2**	**150**	**2.83**	**2.63**	**0.1244**	**1.5**	**1.06**	**0.2148**
12	2000	-2	150	2.82	2.81	0.3153	3.0	3.05	0.3313
13	1000	0	150	1.72	2.72	0.2264	3.0	1.26	0.3500
14	1500	0	150	2.21	2.75	0.1787	2.1	1.13	0.1669
15	2000	0	150	2.28	2.92	0.2720	3.2	2.02	0.3054
16	1000	2	150	1.19	2.77	0.2750	4.3	4.08	0.2205
17	1500	2	150	1.47	2.90	0.1785	2.6	2.28	0.1724
18	2000	2	150	1.78	2.92	0.3124	4.7	5.61	0.1823
19	1000	-2	200	2.10	2.50	0.3557	5.5	4.24	0.4203
20	1500	-2	200	2.14	2.64	0.2685	3.5	4.14	0.2950
21	2000	-2	200	2.38	2.73	0.1780	2.2	1.74	0.2446
22	**1000**	**0**	**200**	**1.75**	**2.76**	**0.1193**	**1.9**	**1.37**	**0.1441**
23	1500	0	200	2.05	2.62	0.2367	3.6	0.94	0.2744
24	**2000**	**0**	**200**	**2.14**	**2.91**	**0.1283**	**1.6**	**1.00**	**0.2809**
25	1000	2	200	1.34	2.41	0.2914	5.5	0.23	0.2439
26	1500	2	200	1.52	2.64	0.1964	3.5	0.60	0.1126
27	2000	2	200	1.48	2.76	0.1530	2.5	2.48	0.1417

3.2. ANOVA

A factorial three-way ANOVA with confidence value of 0.05 and degrees of freedom of 2 for each factor and 4 for each factor interaction was conducted to compare the main effects of P_r, A_z and f as well as their interaction effects on the quality of the weld by analyzing the total pore area of the weld (*tpa*), porosity area (A_p) and maximum observed pore diameter (D_p). The analysis is testing the hypothesis that the samples within the setup are having the same mean against the alternative hypothesis that means are not all the same: if p-value is higher than 0.05 the hypothesis is accepted, therefore the variation of the tested parameter(s) has no

statistically significant effect on the investigated output. The results are shown in Table 5, statistically significant effects are highlighted.

Table 5. Experimental results: factors and p-values

Factors	*tpa*, mm²	A_p, %	max D_p, mm
Ring laser power (P_r)	0.1948	**0.0150**	0.2551
Focal point position offset (A_z)	**0.0368**	**0.0142**	**0.0362**
Frequency (f)	0.3998	0.8796	0.8134
$P_r \cdot A_z$	0.2633	0.1338	0.4589
$P_r \cdot f$	0.0579	**0.0405**	0.3405
$A_z \cdot f$	0.8853	0.5642	0.2539

As shown in the table, A_z was statistically significant at $p \leq 0.05$ for all investigated porosity outputs. The main effect of P_r was statistically significant on A_p at $p = 0.0150$. These results indicated that the ring laser power has an effect on the porosity area, possibly through the stabilization of the keyhole. The examination of this possible explanation require high-speed camera observation of the weld pool (same method have been used by Sokolov et al., 2021) to confirm the increased stability (i.e. reduction of fast fluctuations of the keyhole opening during welding) of the process at selected parameters. With one exception, on the whole, the interaction effects were not significant, indicating that there was no combined effects of P_r and A_z, A_z and f. Hence, only the interaction effect of P_r and f was statistically significant on A_p at $p = 0.0405$ while f as a single factor had no significant influence on the porosity outputs. The joint effect of the dual beam welding and high frequency beam oscillation has a significant effect on A_p.

3.3. Tensile tests

The result of joint strength testing the parameters of experiment 24 are shown in Fig. 5. The output shows average result of 120 MPa ultimate tensile strength. In all tests, the fracture was located in the center of the weld surface. Fracture initiation located in the higher stress concentration, i.e., on the weld border of the interface. That can be explained by the specifics of the lap shear tensile test in fillet lap joint setup. In case of static stress, porosity on the way of possible fracture weakens the joint. Experiment 24 cross sections were not showing any pores around the interface non-welded area (Fig. 5, (c) - stress concentration zone).

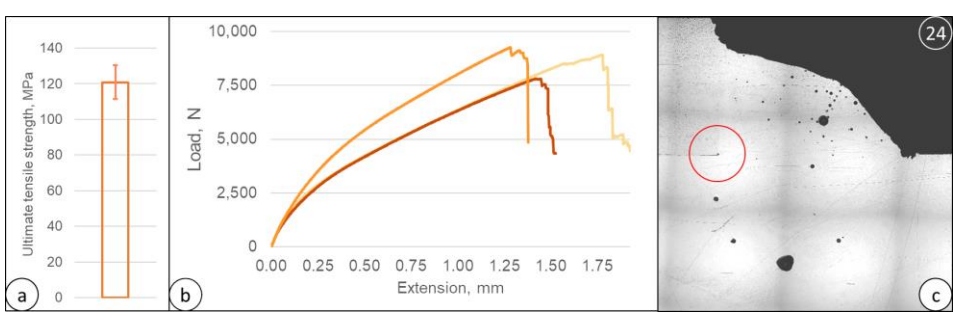

Fig. 5. Tensile tests results: (a) ultimate tensile strength; (b) load to extension plot for tested samples; (c) experiment 24 cross section with stress concentration zone on the weld border marked with red circle

However, it can be assumed that the increase in pore formation around the high stress concentration zone can significantly reduce the tensile strength and fatigue properties of the weld.

4. Conclusions

The paper discussed challenges and technological solutions of remote laser welding of die casting aluminum C611 to aluminum extrusion AA6063 in fillet lap welding setup. Key findings are listed below:

- Weld porosity can be reduced by combination of dual-laser beam and frequency beam oscillation. The reduction of porosity below 2% (1.6% average) of the weld area achieved with oscillation frequency (f) = 200 Hz, position offset (A_z) = 0 mm (on the surface of the top plate), ring laser power (P_r) = 2000 W with constant speed 66.67 mm/sec (4 m/min) with applied power modulation of the core laser power.
- Tensile test results show average 120 MPa ultimate tensile strength.

Future work will be devoted to study other weld joint configurations and material sets with die casting aluminum with application of weld porosity reduction methods discussed in the article. Further research should be undertaken to investigate the physical phenomenon underlying the porosity reduction. A possible solution can be high speed camera observations of the weld pool to evaluate the effects of beam oscillation and ring laser on stabilization of the keyhole.

Acknowledgment

This study was partially supported by (1) APC UK project: Chamaeleon: “New lightweight Materials and Processing Technologies for Common Lightweight Architecture of Electric and Hybrid Powertrain Systems”; (2) Innovate UK IDP15 project LIBERATE: “Lightweight Innovative Battery Enclosures using Recycled Aluminium Technologies”; (3) WMG HVM Catapult.

References

Ceglarek, D., Colledani, M., Váncza, J., Kim, D. Y., Marine, C., Kogel-Hollacher, M., Mistry, A., Bolognese, L., 2015. Rapid deployment of remote laser welding processes in automotive assembly systems. CIRP Annals, 64(1), p. 389-394.

Dittrich, D., Jahn, A., Standfuss, J., Beyer, E., 2017. Laser beam welding of atmosphere aluminum die cast material using high frequency beam oscillation and brilliant beam sources. Journal of Laser Applications, 29(2), paper 0224225.

Franciosa, P., Serino, A., Al-Botros, R., & Ceglarek, D., 2019. Closed-loop gap bridging control for remote laser welding of aluminum components based on first principle energy and mass balance. Journal of Laser Applications, 31(2), paper 022416.

Gullino, A., Matteis, P., D’Aiuto, F., 2019. Review of aluminum-to-steel welding technologies for car-body applications. Metals, 9(3), p. 315.

Hong, K. M., Shin, Y. C., 2017. Prospects of laser welding technology in the automotive industry: A review. Journal of Materials Processing Technology, 245, p. 46-69.

Kumar, R. R., Alok, K., 2020. Adoption of electric vehicle: A literature review and prospects for sustainability. Journal of Cleaner Production, 253, paper 119911.

Maina, M., Okamoto, Y., Okada, A., Närhi, M., Kangastupa, J., Vihinen, J., 2018. High surface quality welding of aluminum using adjustable ring-mode fiber laser. Journal of Materials Processing Technology, 258, p. 180-188.

Müller, A., Goecke, S. F., Sievi, P., Albert, F., & Rethmeier, M., 2014. Laser beam oscillation strategies for fillet welds in lap joints. Physics Procedia,, 56, p. 458-466.

Sokolov, M., Franciosa, P., Sun, T., Ceglarek, D., Dimatteo, V., Ascari, A., Fortunato, A. & Nagel, F. 2021. Applying optical coherence tomography for weld depth monitoring in remote laser welding of automotive battery tab connectors. Journal of Laser Applications, 33(1), paper 012028.

Sun, T., Franciosa, P., Sokolov, M., & Ceglarek, D., 2020. Challenges and opportunities in laser welding of 6xxx high strength aluminium extrusions in automotive battery tray construction. Procedia CIRP, 94, p. 565-570.

Wang, L., Mohammadpour, M., Yang, B., Gao, X., Lavoie, J., Kleine, K., Kovacevic, R., 2020. Monitoring of keyhole entrance and molten pool with quality analysis during adjustable ring mode laser welding. Applied Optics, 59(6), p. 1576-1584.